Available online at www.sciencedirect.com
SCIENCE DIRECT®
International Journal of Plasticity 21 (2005) 1640–1657
INTERNATIONAL JOURNAL OF Plasticity
www.elsevier.com/locate/ijplas

An investigation of the effects of solution heat treatment on mechanical properties for AA 6xxx alloys: experimentation and modelling

R.P. Garrett, J. Lin *, T.A. Dean

Mechanical and Manufacturing Engineering, School of Engineering, University of Birmingham, Edgbaston, Birmingham B15 2TT, UK

Received in final revised form 20 April 2004
Available online 19 December 2004

Abstract

A series of thermal-mechanical tests have been designed and carried out on the aluminium alloy AA 6082 to investigate the effects of solution heat treatment (SHT) time on the mechanical properties for a range of deformation rates at the SHT temperature of 525 °C. Particularly the effects of SHT time on the flow stress, ductility and anisotropy of the material are investigated experimentally. Based on Pearl's growth rate equation and diffusion theory, a SHT completeness variable is introduced to model the microstructural evolution of the material during the SHT period. This SHT evolution variable is incorporated into a viscoplastic material model to simulate the material flow at different levels of SHT completeness. A new set of unified SHT viscoplastic constitutive equations is formulated and the constants within the equation set are determined from the experimental data of AA 6082, using an Evolutionary Programming (EP) based optimisation software package. Further experimental work has been carried out for different deformation and SHT conditions to validate the model predictions.

Keywords: Materials modelling; Solution heat treatment; Hot forming; Viscoplastic SHT model; Aluminium alloys

* Corresponding author. Tel.: +44 0121 414 3317; fax: +44 0121 414 3958.
E-mail address: j.lin@bham.ac.uk (J. Lin).

0749-6419/$ - see front matter
doi:10.1016/j.ijplas.2004.11.002

1. Introduction

Within the automotive industry there is an ever-increasing demand for the use of sheet aluminium alloy components, mainly due to their high strength to weight ratio (when fully thermally treated) in comparison to steels (Miller et al., 2000; Engler and Hirsch, 2002; Polmear, 2000). These alloys also provide good dent resistance, which is of extra benefit to automotive body panel applications (Engler and Hirsch, 2002). Automotive components often require complex shaped designs with high strength. At present the required material properties are achieved by thermally treating the material (Engler and Hirsch, 2002). This thermal treatment consists of three main processes: (1) SHT: this is where the material is held at an elevated temperature for a sufficient time, so that all the constituents are taken into solid solution, giving one single phase. (2) Quenching: this is when the material is rapidly cooled from the SHT temperature to room temperature so as to 'freeze' this super-saturated state within the material at room temperature, giving a microstructure condition known as 'Super Saturated Solid Solution' (SSSS). (3) Ageing: age-hardening is the final stage in the development of the properties of heat treatable alloys, it is the controlled decomposition of the SSSS to form finely dispersed precipitates (Ho et al., 2003; Gracio et al., 2004). Some alloys undergo ageing at room temperature (natural ageing), but most require heating for a time interval at one or more elevated temperatures (artificial ageing) (Yoon et al., 2004).

Once the material has been thermally treated and modified to the required mechanical properties, the next stage is to form the material into the component shape. This stage can often be difficult in the manufacture of automotive sheet components, due to the post-aged high strengths and low ductility of the workpiece material (Aluminium Federation, 1993; Khaleel et al., 1998). These properties can result in forming difficulties, such as the inability to achieve high drawing depths and tight bending radii (i.e., sharp corners), etc. The cause of these problems is mainly due to low ductility, and this must be improved in order to manufacture the wide range of features commonly found in automotive components (Bolt and Lamboo, 2001). Springback is also a common occurrence when forming high strength sheet aluminium alloys.The usual solution to the ductility and springback problems when manufacturing such components is to hot form the component, i.e., form at an elevated temperature (Li and Ghosh, 2003, 2004). This allows a reduction in flow stress and an improvement in the formability of the material. Even though hot forming solves these particular problems, it has the potential to generate a number of additional problems. One serious effect is the 'thermally enhanced' mechanical properties of the material being destroyed or severely reduced due to the exposure at high temperature. It is therefore of advantage if forming is completed at a time prior to any thermal strengthening of the material.

When observing the aluminium alloy, it is known that the ductility of the material is obtained from the SHT stage of the T4 treatment, and the strength is obtained from the ageing process of the T6 treatment (Engler and Hirsch, 2002). It is thus proposed in this paper that the forming process should be completed prior to age hardening of the material. Zhang et al. (2002) have experimentally shown that enhanced

ductility is achievable when the material is fully SHTed. Test results on solid bars of a 6xxx aluminium alloy showed the SHT effects level off once beyond a given SHT time. Beyond this 'time barrier' there is little change in the material strength and ductility, hence the optimum mechanical properties have been achieved. These tests provide evidence that the mechanical properties change in relation to the SHT time, but no modelling has been done and insufficient experimental data was given in the paper to provide calibration for the creation of a complete SHT effect model.

At present most models that consider the effect of precipitation on the final material properties are those observing the growth of precipitates during ageing (Esmaeili et al., 2001, 2003a,b; Myhr et al., 2001). Each of these models considers the inputs of strength from a number of factors such as the aluminium matrix, solid solution and precipitates of each phase variety. These models define the strength variation due to different proportions of each input fairly well. Such properties include the volume fraction of the precipitates at each stage. There is a need to link the SHT time proportion with the yielding strength and observe these effects. Thus, the main aim of the research described in this paper is to experimentally obtain further data in terms of stress–strain relationships for a variety of SHT time proportions, deformed at a range of strain rates. The effect of anisotropy will also be tested to see if this material property holds in the fully SHTed condition (Lopes et al., 2003; Wu et al., 2003). Using this collection of experimental data a new set of constitutive equations to model the SHT effect on the yield stress of a material are developed, and incorporated into a viscoplastic material model.

2. Mechanisms of SHT for 6xxx aluminium alloys

SHT is the thermal process in which the material is held at the SHT temperature (T_{SHT}) for a given time until the alloying elements are fully taken into the solid solution. At the start of SHT the alloying elements of the aluminium alloys are in 'clusters', usually known as precipitates. For 6xxx series aluminium alloys, these precipitates are made up mainly of Mg_2 Si and/or Si. Such precipitates are present in the alloy due to the pre-treatments of the sheet material during forming, SHT and ageing processes, carried out prior to receiving the material. As discussed in Section 1, the SHT process is split into three stages. During the third stage (age-hardening), precipitates (secondary phases) are allowed to grow at an increased rate due to the elevated temperature of the artificial ageing process. The presence of these precipitates increases the strength of the material, but reduces the ductility.

At the start of the treatment the solutes are in patches of highly concentrated alloying elements (precipitates) of different size that provide barriers to the flow of the material during deformation (Fig. 1(a)). With time these precipitates dissolve into the material, diffusing throughout the whole structure (Figs. 1(b) and (c)). This diffusion results in the 'flow barrier' being reduced and eliminates the chance of forming micro-voids around second phases in plastic deformation (Gelin, 1998; Glazoff et al., 2004; Hu et al., 2004). This results in the ductility being increased and the flow stress being reduced when hot tensile tested. Holding the material at the SHT

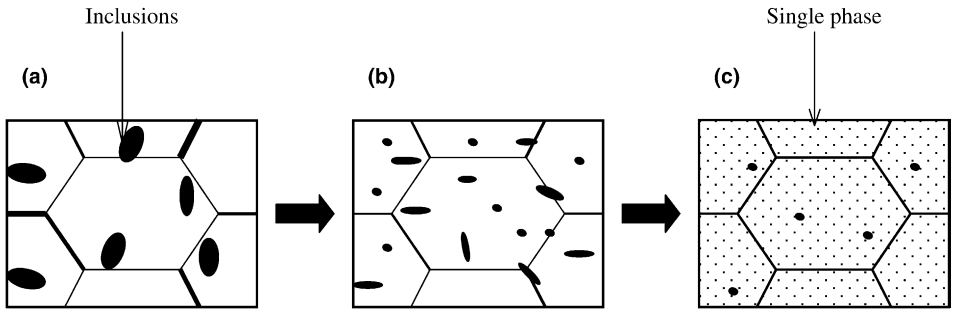

Fig. 1. Schematic diagram showing the microstructure evolution for the material: (a) at the beginning of SHT; (b) intermediate SHT; (c) close to finishing SHT.

temperature (T_{SHT}) for the required time will also allow such factors as irregular precipitates and residual stresses to be further reduced, giving a more homogeneous microstructure throughout the whole material, and hence a more formable material. As the time passes further diffusion of the alloying elements happen and features such as coarsening, rounding and transforming occur as well as the dissolution of Mg_2 Si phases. This rounding off of hard non-dissolvable particles with sharp edges also improves the ductility and reduces the occurrence of holes when thin walled products are formed (Engler and Hirsch, 2002; Dons, 2001). The essential premise for the diffusion of the alloying elements during SHT is the solubility within the aluminium matrix (Chen et al., 1999; Vermolen and Van der Zwaag, 1996; Vermolen and Vuik, 2000). The rate of dissolution is proportional to the SHT temperature T_{SHT} right up to the solidus of the alloy and it is thus clearly beneficial to carry out the SHT as close as possible to the solidus of the alloy (Varley, 1970). But the maximum temperature must never be higher than the solidus, because of the risk of the material melting which will enable unwanted microstructural features to occur. Sufficient time must be given to completely re-dissolve the second phase, the duration of soaking is determined by the rate of dissolution of strengthening elements (smaller finer precipitates dissolve at a faster rate) and the nature of the alloys.

3. Experimental programme

The heat treatable aluminium alloy, AA 6082 was supplied in large sheets with a thickness of 1.5 mm, the sheet alloy was in a T6 condition i.e., SHTed, quenched, stretched (3%) in the rolling direction, then artificially aged. The recommended SHT conditions for such a material are to heat it at 525 °C for 30 min (Aluminium Federation, 1993), which ensures the full dissolution of the alloying elements into the aluminium matrix. This is a typical process for producing commercial AA6XXX aluminium alloy sheets. If the material is only hot or cold rolled, the stress–stain relationships at the initial stage of the solution heat treatment would be different, which will be discussed in the later sections.

The tensile tests were carried out mainly in the rolling direction. To investigate the effect of SHT time on anisotropy, additional tests were conducted in the direction perpendicular to rolling for a number of selected test conditions. Thermocouples were attached to testpieces to control the test temperature. Tests were carried out at different SHT completeness while at the T_{SHT} using a Gleeble Material Simulator. Fig. 2(a) shows the temperature control and the experimental procedure. To avoid the possibility of overshoot in temperature, the heating phase is divided into two steps; the first step is to heat the testpieces to 500 °C using a heating rate of 50 °C/s (0A), the remaining heating is completed at a rate of 2.5 °C/s (AB). The material was then held at the SHT test temperature of 525 °C for a given time (BC), before deforming the testpiece until failure (CD).In the tests, the following aspects were considered: (i) the holding time before deformation takes place (BC) at the T_{SHT}

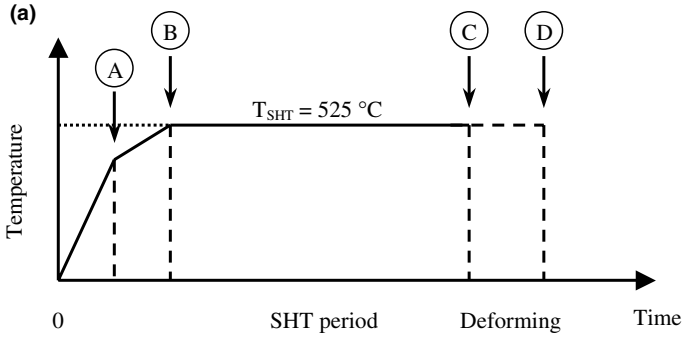

(b)

$\dot{\varepsilon}$ (s^{-1}) \ SHT Time proportion	0	0.33	0.66	1.0
0.01	+		+	
0.1	+	+	+	+
1.0	+	+	+	+
10.0	+		+	

Fig. 2. (a) Schematic diagram showing the experimental conditions. (b) Test planning diagram. '+' represents that the tests are carried out at those conditions in the rolling direction. SHT time proportion is defined by (The time between BC in Fig. 2(a)) – (Full SHT time). The tests in the shaded region are used for validating modelling results.

(i.e., 0, 10, 20 and finally 30 min), (ii) the strain rates at which the material was deformed until failure (CD) (i.e., 0.01, 0.1, 1.0 and 10 s^{-1}), and, (iii) the orientation of testpieces (in the direction of rolling and perpendicular to rolling). The experimental conditions for the material tested in the rolling direction are summarised in Fig. 2(b) and those that have been done are shown with a '+' symbol. The SHT time proportion is defined by (The time between BC in Fig. 2(a)) divided by (Full SHT time), where the full SHT time is 30 minutes (Aluminium Federation, 1993).

4. Experimental results

4.1. Effects of SHT time on flow stress

Symbols in Fig. 3 show the experimental results of the material tested at SHT time proportions of 0.0, 0.33 and 1.0 for two strain rates of 0.1 s^{-1} (Fig. 3(a)) and 1.0 s^{-1} (Fig. 3(b)). Lower flow stresses are observed for higher SHT time proportions at both strain rates, this is due to more precipitates or inclusions being dissolved for longer SHT times. For a strain rate of 0.1 s^{-1} the steady state flow stress is reduced by around 24% (Fig. 3(a)) by increasing the SHT time proportion from zero to one. Similar results are observed for the higher strain rate, 1.0 s^{-1} (Fig. 3(b)). In this case there is around 20% drop in steady state flow stress for the same SHT proportion. This shows that forming the materials with higher SHT time proportions requires lower loads and thus less powerful presses can be used, this provides major benefits in terms of the financial savings.

Symbols in Fig. 4 show the strain rate dependent flow stresses for different SHT time proportions: 0.0 and 0.66. Although the magnitudes of flow stresses are different for the different SHT proportions the material exhibits the same strain rate sensitivity behaviour. The flow stresses at the steady state increase by about 30% as the strain rate increases from 0.01 to 10 s^{-1} for both SHT time proportions. Those test results provide the basic information for the modelling of the effects of SHT in relation to the mechanical properties of the material.

Fig. 5(a) shows the relationship between maximum flow stresses and SHT time proportion for the material tested at strain rates of 0.1 and 1.0 s^{-1}. The solid lines are the experimental results obtained in the rolling direction and these show that the maximum flow stress drop rate reaches a peaks at the SHT time proportion of about 0.4 for both cases. The maximum flow stress keeps approximately the same magnitude when the SHT time proportion is greater than 0.65, at this proportion almost all the particles/inclusions are believed to be dissolved into the aluminium matrix. The difference of the maximum flow stress between zero and maximum SHT is around 30% for both strain rates.

4.2. Effects of SHT time on ductility

Solid lines in Fig. 5(b) show the experimental results of the material tested at SHT proportions of 0.0, 0.33, 0.66 and 1.0 at strain rates of 0.1 and 1.0 s^{-1}. Lower

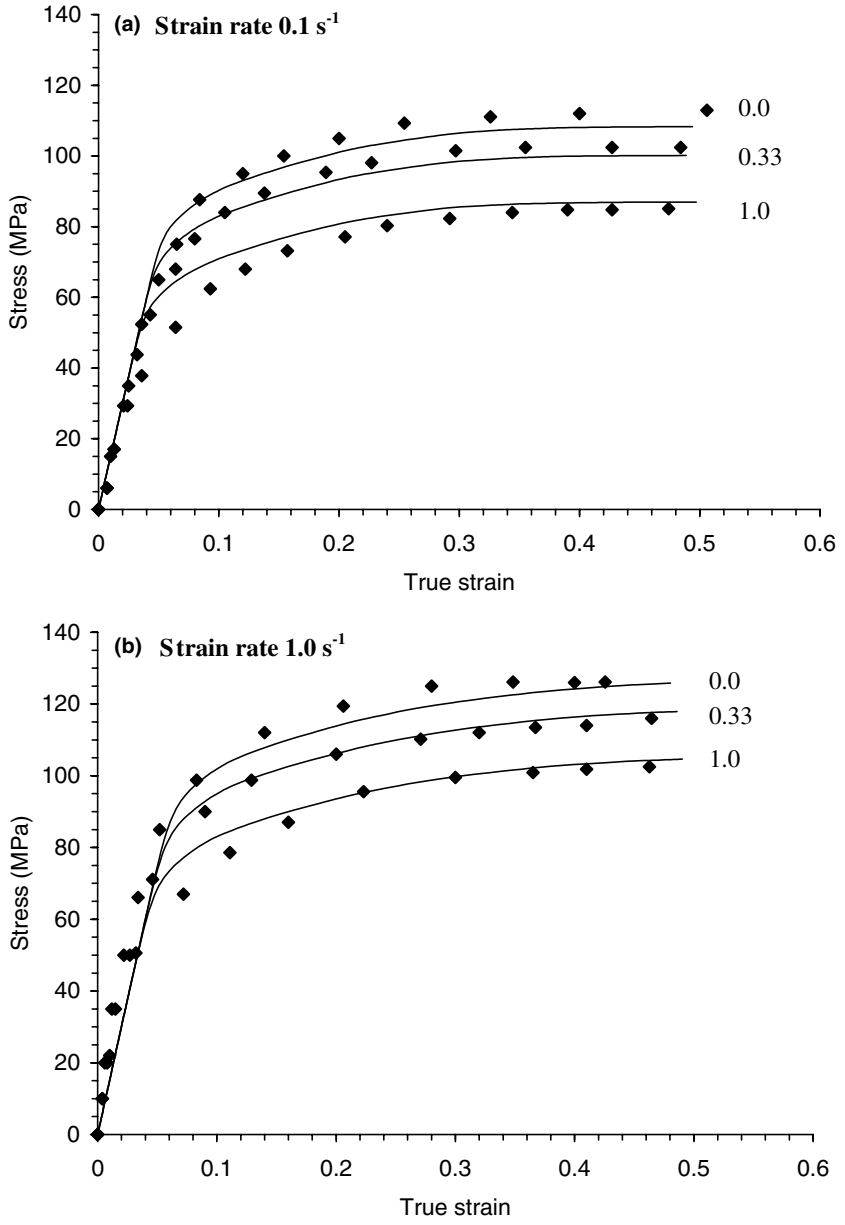

Fig. 3. Comparison of experimental (symbols) and (a) computed (solid curves), (b) predicted (solid curves) stress–strain relationships for different SHT time proportions: 0.0, 0.33 and 1.0 at $\dot{\varepsilon} = 0.1$ and 1.0 s^{-1}.

ductility is observed for lower SHT time proportions for both strain rates. It can be seen that an increase of around 22% can be achieved by fully treating the material for both strain rates. This increase in ductility is mainly due to a reduction in the barriers

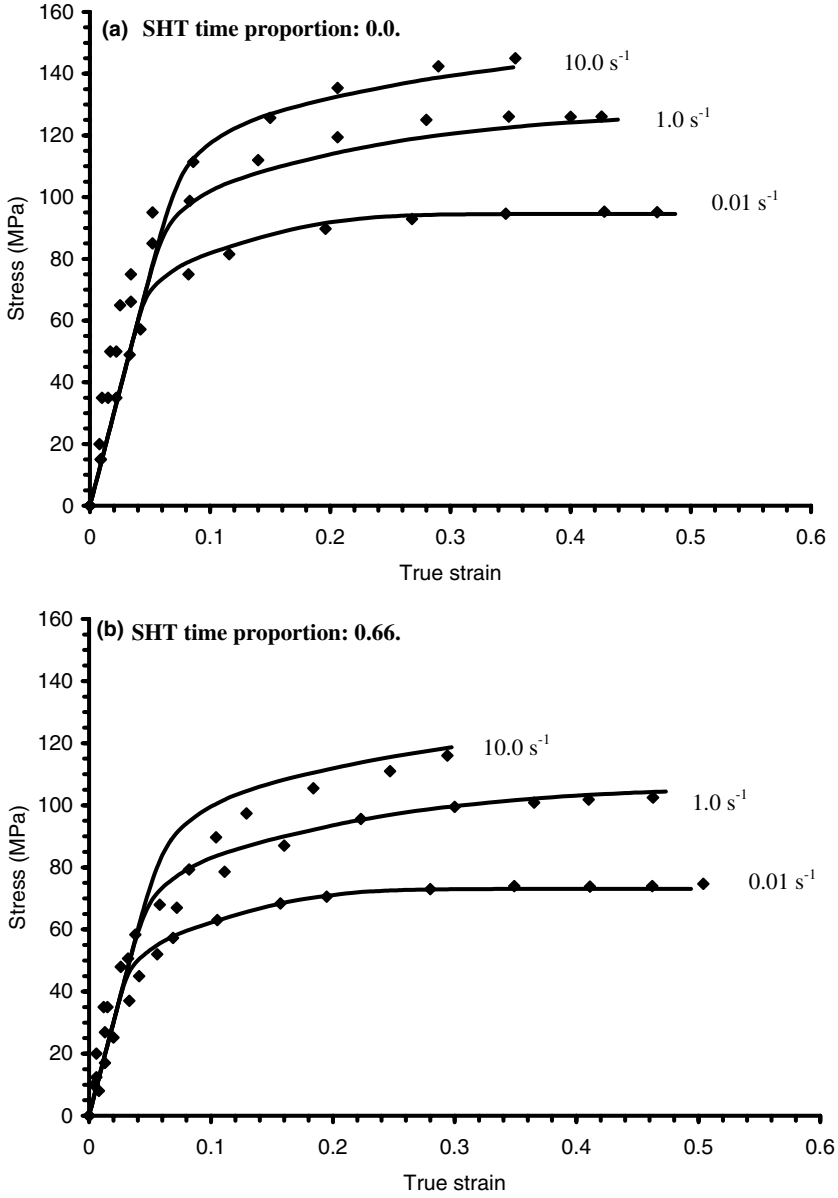

Fig. 4. Comparison of experimental (symbols) and computed (solid curves) stress–strain relationships for different strain rates at: (a) 0.0; (b) 0.66 SHT time proportions.

to flow that affect the steady state flow stress discussed in Section 4.1. Strain rate was also shown to have a direct affect on the magnitudes of ductility for all SHT time proportions. Lower strain rates are shown to allow higher levels of ductility to be

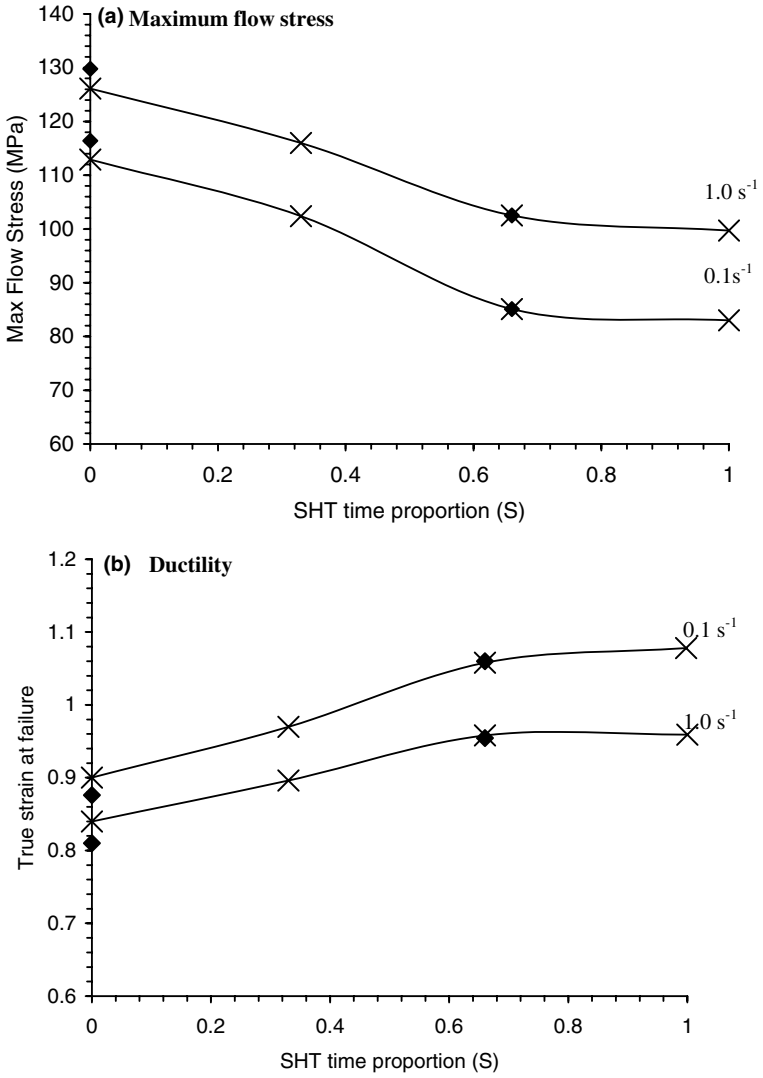

Fig. 5. Comparison of: (a) the maximum flow stress; (b) the ductility with different SHT time proportions for the testpieces cut in the directions of rolling (∗) and perpendicular to the rolling (V).

achieved, this was due to the slower strain rates giving the microstructure more opportunities to respond to the deformation in terms of such mechanisms as atomic slip. If increased ductility can be achieved during presswork, then more complicated components can be manufactured with such features as large draw depths and sharp corners. The ability to form components of higher complexity will enable smaller components to be combined into larger more complicated components. This will

reduce the number of parts to be manufactured and thus allow considerable weight reduction in such automotive applications.

4.3. Effects of SHT time on anisotropy

Symbols in Fig. 5 shows test results obtained in directions perpendicular to and normally to rolling. For no SHT the maximum flow stress in the rolling direction is about 5% lower than that in the normal directions (Fig. 5(a)). Although the ductility is higher as the SHT time proportion reaches around 0.66, the directional differences in both maximum flow stresses and ductility disappear. This indicates that the directional difference of the microstructure of the material due to pre-processing gradually fades out during the SHT. When the material is fully SHTed the anisotropic material becomes isotropic. This would make the control of the forming process easier.

5. Development of unified SHT viscoplastic constitutive equations

5.1. Modelling the effects of SHT on the mechanical properties

Throughout the process of SHT, the microstructure of the material is modified. This results in dynamic changes of mechanical properties of the material. This process continues until the 20 min time boundary, where the aluminium and its alloying components are said to be within the SSSS stage (Fig. 1(c)). This is where the alloying elements are finely dispersed throughout the whole aluminium microstructure.

It can be seen from the experimental results shown in Fig. 5(a) that as SHT time proportion increases, the maximum flow stress decreases until the 0.66 level but once beyond this level the changes are minimal. The yield stress/elastic limit of the material is shown to follow the same trends during the SHT and thus will be considered in the SHT viscoplastic model. Due to this aspect of diffusion during the dissolution of alloying elements it is necessary to include a diffusion factor in the SHT equation. From Porter and Easterling (2001), it is known that this diffusion process can be described as,

$$D = D_0 \exp\left(-\frac{Q}{R_{GC} T_{SHT}}\right). \tag{1}$$

The diffusion parameter D is a temperature dependent feature, which allows for the effect of increasing diffusion rate for increasing temperature, necessary in a SHT model. D_0 is the diffusion coefficient, Q is the activation energy, T_{SHT} is the SHT temperature and R_{GC} is the universal gas constant. The evolution of SHT is therefore related to the diffusion parameter.

$$\dot{S} = f(D, S). \tag{2}$$

The variable S represents the completeness of SHT and models the dissolution of the alloying elements into the aluminium matrix. At the beginning of the SHT process

$S = 0.0$, and when the material is fully SHTed, $S = 1.0$. To model the microstructural evolution of the SHT, the following rate equation is introduced

$$\dot{S} = D(1 - S)^{n_3}, \tag{3}$$

where n_3 is a material constant used to control the rate of increase of the SHT effect.

The completeness of SHT directly affects the flow stress of the material. This is clearly seen in the experimental results shown in Fig. 5(a), and can be modelled using a modified form of the Pearl's growth rate equation (Vadasz and Vadasz, 2002).

$$\dot{P} = ry\left(\frac{L - y}{L}\right), \tag{4}$$

where $\dot{P}$ is the rate of increase of population per unit of time (s^{-1}), in our case the population is related to the quantity of un-dissolved alloying elements, L is the maximum sustainable population and is directly related to y, the population size factor. This size factor has a similar meaning to the SHT completeness variable S. The factor r is the growth rate constant. Fig. 6 shows the typical S-shaped growth curve (Vadasz and Vadasz, 2002), with an initial plateau (AB) followed by a sharp increase in rate (BC), and a secondary plateau (CD) at the maximum population.

To model the SHT – yield stress relationship it is necessary to replace the population size factor (y) with the SHT 'completeness' function (S). This allows the SHT effect to be directly linked with the reduction in the population or quantity of un-dissolved alloying elements. Due to the maximum population (maximum SHT completeness value) being equal to 1, L in Eq. (4) will be substituted with the number 1. To adapt the equation it is also necessary, to reverse the Pearl's Growth Curve, so the population or quantity of un-dissolved alloying elements is high at the start and reduces until it reaches a constant minimal point, it is therefore necessary to introduce a negative sign in front of Eq. (4). The population factor is replaced with the yield stress variable, thus the relationship can be simplified by Eq. (5), when $L = 1$,

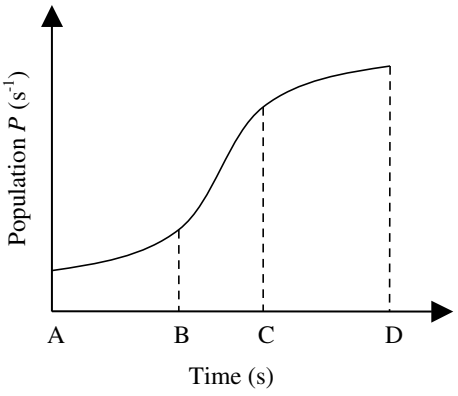

Fig. 6. Pearl's population growth curve showing the dissolution of alloying elements into the aluminium matrix during the SHT process (Vadasz and Vadasz, 2002).

$$\dot{\sigma}_y \propto -\dot{P}. \tag{5}$$

By considering the SHT parameters and substituting Eq. (4) into Eq. (5), the evolution of yield stress during the SHT period can be expressed as,

$$\dot{\sigma}_y = -rS(1-S)^{n_4}. \tag{6}$$

This equation can be coupled with Eq. (3) and used to model the yield stress evolution of a given material in relation to the completeness of SHT. The addition of the material constant, n_4, is to provide a higher level of control over the whole equation.

5.2. The unified constitutive equations

Viscoplastic constitutive equations have been developed by many researchers for many engineering materials (Vadasz and Vadasz, 2002; Lin et al., 2002; Lin and Liu, 2003; Lin, 2003; Trivedi et al., 2004; Celentano, 2002), and have been used to model a wide range of time dependent phenomena, such as strain rate effects, creep, recrystallisation, recovery, etc. In those equations, hardening of a material during viscoplastic deformation is modelled according to the accumulation of plastic strains only (Lin, 2003; Lin et al., 1996). Recently dislocation-based hardening constitutive equations have been developed by Lin and Liu (2003), and Lin (2003), where the recovery of dislocations due to annealing and recrystallisation in hot forming conditions is included. By implementing the SHT variable and the yield stress evolution equations into the dislocation-based viscoplastic material model omitting the recrystallisation and grain growth variables, a new set of unified SHT viscoplastic constitutive equations can be formed, which is given below:

$$\begin{aligned}
\dot{\varepsilon}_{\mathrm{p}} &= \left(\frac{\sigma - R - \sigma_y}{K}\right)^{n_1},\\
\dot{S} &= D(1-S)^{n_3},\\
\dot{\sigma}_y &= -rS(1-S)^{n_4},\\
\dot{R} &= \frac{1}{2}B\rho^{-1/2}\dot{\rho},\\
\dot{\rho} &= A(1-\rho)\left|\dot{\varepsilon}_{\mathrm{p}}\right| - C\rho^{n_2},\\
\sigma &= E(\varepsilon_T - \varepsilon_{\mathrm{p}}),
\end{aligned} \tag{7}$$

where $\dot{\varepsilon}_{\mathrm{p}}$ in the Eq. (7) is the traditional power law viscoplastic flow formulation with difference of the yield stress σ_y of the material dynamically changing during the SHT period. According to the nature of this practice, the material is firstly SHTed for a given period then deformed, the numerical procedure is therefore divided into two steps. The first step is to integrate the SHT equation $\dot{S}$ and the yield stress evolution equation $\dot{\sigma}_y$, with initial values (when $t = 0$) of $S = 0$ and $\sigma_y = \sigma_0$, where σ_0 is the initial yield stress of the material at the SHT temperature. Once the deformation takes place after a given SHT time, the other equations within Eq. (7) are included in the integration. The effect of the viscoplastic

deformation on the SHT variable S is omitted here, since the deformation rate in practical metal forming processes are high and the time for the deformation period is short.

The material hardening R due to the plastic deformation is calculated according to the accumulation of dislocation density ρ (Lin and Liu, 2003,Lin, 2003). The first part of the dislocation density rate $\dot{\rho}$ equation represents the accumulation of the dislocation density due to plastic flow of the material ($|\dot{\varepsilon}_p|$) and the dynamic recovery. The second term in the equation describes the static recovery of dislocations due to annealing. The detailed descriptions of the dislocation hardening equations have been reported by Lin and Liu (2003); Lin (2003). K, n_1, B, n_2, n_3, D, r and n_4 are material constants, which are determined from experimental data using the EP-based optimisation method described in the next section. E is the Young's modulus of the material and $E = 1000$ MPa (Lin et al., 2002).

6. Determination of the unified material model for AA 6082

Extensive research has been carried out on the development of Evolutionary Algorithm (EA) based optimisation techniques in materials modelling (Lin and Liu, 2003; Lin, 2003; Li et al., 2002) and computer software system has been developed specifically to solve such non-linear optimisation problems (Lin and Yang, 1999). To determine these material constants, the formulation of an objective function for this particular problem is necessary which can work efficiently with the experimental data. An objective function obtained from Lin et al. (2002) is given.

$$f(x) = \sum_{j=1}^{M} \sum_{i=1}^{N_j} \left\{ \omega 1_{ij} \left[\frac{\sigma_{ij}^{e} - \sigma_{ij}^{c}}{\alpha \sigma_{N_j j}^{e}} \right]^2 + \omega 2_{ij} \left[\frac{\varepsilon_{ij}^{e} - \varepsilon_{ij}^{c}}{\alpha \varepsilon_{N_j j}^{e}} \right]^2 \right\}, \tag{8}$$

where $\omega 1_{ij} = \sigma_{ij}^{e} / \sum_{j=1}^{M} \sum_{i=1}^{N_j} \left(\sigma_{ij}^{e} \right)$ and $\omega 2_{ij} = \varepsilon_{ij}^{e} / \sum_{j=1}^{M} \sum_{i=1}^{N_j} \left(\varepsilon_{ij}^{e} \right)$ are the weighting functions for stress and strain. In the weighting functions, both sum of the weightings are equal to 1, which ensures that the sum of the error is also normalised against the number of data points. M corresponds to the number of experimental curves, and N_j corresponds to the number of data points for the jth experimental curve. σ_{ij}^{e} and ε_{ij}^{e} corresponds to the ith experimental data point for the jth experimental curve, and σ_{ij}^{c} and ε_{ij}^{c} corresponds to the ith computed data points for jth computed curve. α is a scaling factor so that very small curve features can be modelled, this ensures the best possible representations are obtained from each optimisation process. For this particular case $\alpha = 1$. $\sigma_{N_j j}^{e}$ and $\varepsilon_{N_j j}^{e}$ refer to the maximum magnitudes of the experimental stress and strain for the jth experimental curve.

The modelling work is based on the experimental results obtained from the material in the rolling direction, but the model can be applied to all directions when the material is fully SHTed, due to its isotropic nature.

7. Computational results and analysis

The objective function (8) and the SHT viscoplastic material model (7) have been implemented into the EA-based optimisation software package through a user-defined subroutine. The material constants within the Eq. (7) are optimised against the experimental data (symbols) shown in Fig. 3(a), Fig. 4(a) and (b). These sets of data cover a range of strain rates from 0.01 to 10 s^{-1} and SHT time proportions, from 0.0 to 1.0. Those experimental data are believed to be able to characterise the overall mechanical behaviour of the material at different SHT stages and deformation conditions. The optimisation computations were carried out and the determined material constants are listed in Table 1. The solid curves in Fig. 3(a), Figs. 4(a) and (b) are the best-fit curves through the computations. Close agreement is obtained between the experimental and computed stress–strain curves for all the experimental data involved in the optimisation, although consistent errors occur at the initial stage of the deformation. This indicates that creep takes place in the hot deformation at very low stress levels, which is more obvious for low strain rates (Symbols in Fig. 4). Although the proposed material model could predict the strain rate sensitivity, it is not sensitive enough to catch such details at the initial deformation stage. But, in general the proposed unified SHT material model can be used to model the effect of SHT on mechanical properties.

To investigate the reliability of the predictions, further computations were carried out to predict the experimental data (symbols) presented in Fig. 3(b), which are specially designed for the purpose of validation. It can be observed in this figure that the unified SHT viscoplastic material model, together with the material constants listed in Table 1, is able to predict the mechanical properties of the material very well.

The predicted curves in Fig. 7 were obtained using Eq. (7). As discussed in Section 5.2 the equations were numerically integrated, so as to determine the final stress-strain relationships for each SHT time proportion and strain rate condition. During the integration the values of the SHT completeness and yield stress depend on the SHT completeness conditions modelled using Eqs. (3) and (6). Each of the experimental curves in Fig. 3 and Fig. 4 is plotted up until the highest achieved stress i.e., maximum flow stress, from these plots the level of strain that this maximum flow stress occurs can be determined. When predicting the maximum flow stress it is necessary to integrate the equations to this known strain for each condition. These predicted values are then plotted against their corresponding SHT time proportion values, giving the relationship (solid curves) seen in Fig. 7. It can be observed in Fig. 7 that the predicted curves lie fairly close to the experimental data points

Table 1
Material constants determined for Eq. (7)

A (−)	B (MPa)	C (−)	D (s^{-1})	K (MPa)	r (MPa s^{-1})
2.883	55.504	39.966	0.151	43.247	98.253
n_1 (−)	n_2 (−)	n_3 (−)	n_4 (−)	σ_0 (MPa)	
6.229	7.592	0.195	1.671	45.605	

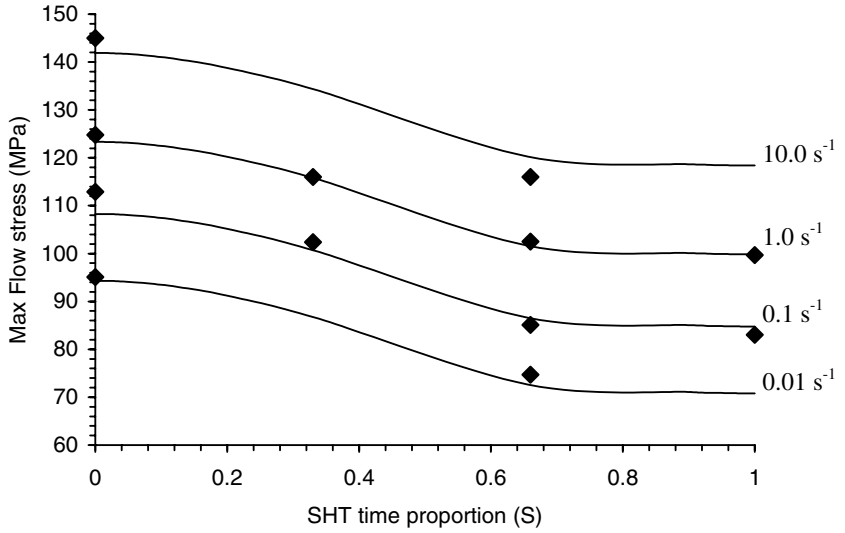

Fig. 7. Comparison of experimental (symbols) and predicted (solid curves) relationship of maximum flow stress and SHT time proportions at $\dot{\varepsilon} = 0.01, 0.1, 1.0$ and $10.0\ s^{-1}$.

(symbols), proving that the equation set can determine the stress–strain and maximum flow stress vs. SHT completeness curves fairly accurately.

The key point, proposed in the work of modelling the effect of SHT on mechanical properties is to predict the effects of SHT time on the yield of the material which is controlled by Eqs. (3) and (6). The diffusion process in the SHT is described by Eq. (1). It varies with SHT temperature, activation energy, alloy content and the initial conditions of a material. Particularly the constant D in Eq. (3) varies with materials and initial processing routes. If Eqs. (3) and (6) are integrated using the constants listed in Table 1 with different magnitudes of D: 0.094, 0.151 and 0.236, the variation of yield stress during the SHT can be obtained and is plotted in Fig. 8. It can be seen that for higher values of D, the influence of SHT on the yield stress is much less. For $D = 0.236$ the yield stress drops by around 33% when fully SHTed. This higher value of D relates to a material with a small initial volume fraction of precipitates. This small quantity of precipitates does not offer much hindrance to flow when untreated, and so when compared to a fully treated sample i.e., precipitates fully dissolved, there is only a small reduction in yield stress. Where as when $D = 0.094$ there is a yield stress reduction of 85%. This can be linked to a material with a large initial volume fraction of precipitates, when SHTed the material evolves from a microstructure with many obstacles to flow to a microstructure with very few boundaries, leading to large changes in the yield stress of the material.

It can be seen in Fig. 8 that at a SHT completeness value of about 0.45, the SHT has a larger effect on the yield stress of the material. At this completeness value the dissolution rate is much higher for smaller values of D. This period of the SHT is therefore the most critical stage of the treatment, and will directly affect the

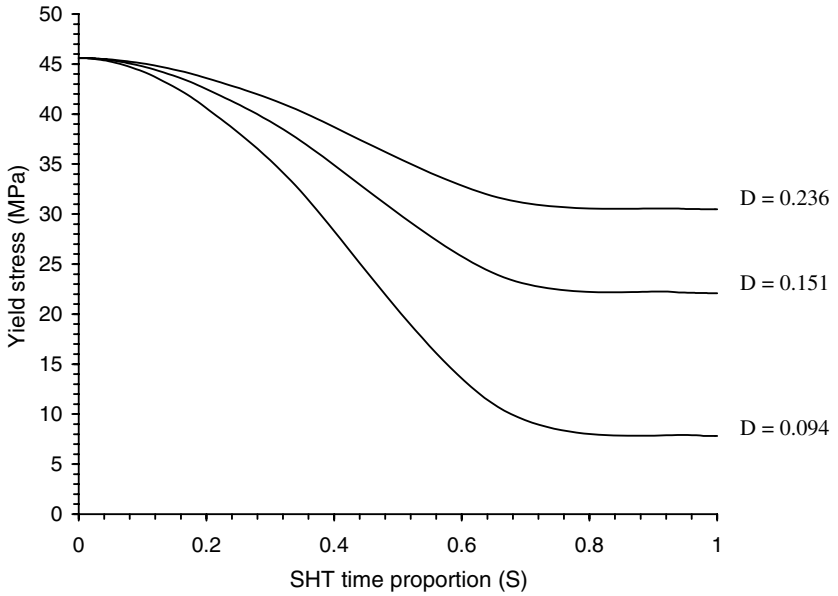

Fig. 8. Prediction of the yield stress variation throughout the SHT process using different values of D.

properties of the material at its fully SHTed state. The value of parameter D depends on microstructure of the material, including grain size and shape, and material processing routes. In this work, the D-value is determined for the aluminium alloy in a T6 condition. If the material is hot rolled, the material will become fully recrystallised during/after the hot rolling process. This results in more uniformly distributed grain size and low dislocation density. Thus, the D-value would be high and the differences of the yield stresses at the beginning and at the end of the SHT would be small. If the material is cold rolled, the grains would be elongated in the rolling direction and the dislocation density would be high (Humphreys and Hatherly, 1996) due to the lack of static recovery and recrystallisation. Thus the D-value would be low and the difference of the yield stress at the beginning and at the end of the SHT would be big.

8. Conclusions

As a result of this research it has been verified by experiments that an increase in ductility and a decrease in maximum flow stress can be achieved by increasing the SHT time proportion. These thermo-mechanical relationships are true for values of SHT time proportion upto 0.66. Above this value the changes in mechanical properties are small in respect to increase SHT time. The experimental results have also shown that when the material is treated beyond the 0.66 SHT time proportions, the initial anisotropy disappears.

Based on experimental observation, a set of novel unified SHT viscoplastic equations have been developed to enable the development of SHT completeness and its effects on the evolution of yield stress of the material to be modelled throughout the SHT process. The combination of these novel equations with a set of viscoplastic constitutive equations enables the effect of SHT on viscoplastic flow to be predicted. This has been verified by experimental results.

References

Aluminium Federation Ltd., 1993. The Properties of Aluminium and its Alloys, ninth ed.

Bolt, P.J., Lamboo, N.A.P.M., Rozier, P.J.C.M., 2001. Feasibility of warm drawing of aluminium products. Journal of Materials Processing Technology 115 (1), 118–121.

Celentano, D.J., 2002. A thermo-mechanical model with microstructure evolution for aluminium alloy casting process. International Journal of Plasticity 18, 1291–1335.

Chen, S.P., Vossenberg, M.S., Vermolen, F.J., Van de Langkruis, J., Van der Zwaag, S., 1999. Dissolution of β particles in an Al–Mg–Si alloy during DSC runs. Material Science and Engineering A 272 (2), 250–256.

Dons, A.L., 2001. The Alstruc homogenisation model for industrial aluminium. Journal of Light Material 1 (2), 133–149.

Engler, O., Hirsch, J., 2002. Texture control by thermomechanical processing of AA 6xxx Al–Mg–Si sheet alloys for automotive applications – a review. Materials Science and Engineering A 336, 249–262.

Esmaeili, S., Cheng, L.M., Deschamps, A.M., Lloyd, D.J., Poole, W.J., 2001. The deformation behaviour of AA6111 as a function of temperature and precipitation state. Material Science and Engineering A 319–312, 461–465.

Esmaeili, S,, Lloyd, D.J., Poole, W.J., 2003a. Modelling of precipitation hardening for the naturally aged Al–Mg–Si–Cu alloy AA6111. Acta Materialia 51, 2243–2257.

Esmaeili, S., Lloyd, D.J., Poole, W.J., 2003b. A yield strength model for the Al–Mg–Si–Cu alloy AA 6111. Acta Materialia 51, 3467–3481.

Gelin, J.C., 1998. Modelling of damage in metal forming processes. Journal of Material Processing Technology 80, 24–32.

Glazoff, V., Barlat, F., Weilanda, H., 2004. Continuum physics of phase and defect microstructures: bridging the gap between physical metallurgy and plasticity of aluminium alloys. International Journal of Plasticity 20 (3), 363–402.

Gracio, J.J., Barlat, F., Rauch, E.F., Jones, P.T., Neto, V.F., Lopes, A.B., 2004. Artificial aging and shear deformation behaviour of 6022 aluminium alloy. International Journal of Plasticity 20 (3), 427–445.

Ho, K.C., Lin, J., Dean, T.A., 2003. Modelling of springback in creep forming thick aluminium sheets. International Journal of Plasticity 20 (4–5), 733–751.

Hu, S.Y., Li, Y.L., Zheng, Y.X., Chen, L.Q., 2004. Effect of solutes on dislocation motion – a phase-field simulation. International Journal of Plasticity 20 (3), 403–425.

Humphreys, F.J., Hatherly, M., 1996. Recrystallization and Related Annealing Phenomena, first ed. Pergamon Press, Oxford.

Khaleel, M.A., Johnson, K.I., Hamilton, C.H., Smith, M.T., 1998. Deformation modelling of superplastic AA 5083. International Journal of Plasticity 14 (10–11), 1133–1154.

Li, B., Lin, J., Yao, X., 2002. A novel evolutionary algorithm for determining unified creep damage constitutive equations. International Journal of Mechanical Sciences 44 (5), 987–1002.

Li, D., Ghosh, A., 2003. Tensile deformation behaviour of aluminium alloys at warm forming temperatures. Materials Science and Engineering A 352 (1–2), 279–286.

Li, D., Ghosh, A., 2004. Biaxial warm forming behaviour of aluminium sheet alloys. Journal of Materials Processing Technology 145 (3), 281–293.

Lin, J., Dunne, F.P.E., Hayhurst, D.R., 1996. Physically-based temperature dependence of elastic viscoplastic constitutive equations for copper between 20 and 500 °C. Philosophical Magazine A 74 (2), 655–676.

Lin, J., Yang, J., 1999. GA based multiple objective optimisation for determining viscoplastic constitutive equations for superplastic alloys. International Journal of Plasticity 15, 1181–1196.

Lin, J., Cheong, B.H., Yao, X., 2002. Universal multi-objective function for optimising superplastic-damage constitutive equations. Journal of Materials Processing Technology 125–126, 199–205.

Lin, J., Liu, Y., 2003. A set of unified constitutive equations for modelling microstructure evolution in hot rolling deformation. Journal of Material Processing Technology 143–144, 281–285.

Lin, J., 2003. Selection of material models for predicting necking in superplastic forming. International Journal of Plasticity 19 (4), 469–481.

Lopes, A.B., Barlet, F., Gracio, J.J., Ferreira-Duarte, J.F., Raunch, E.F., 2003. Effect of texture and microstructure on strain hardening anisotropy for aluminium deformed in uniaxial tension and simple shear. International Journal of Plasticity 19, 1–22.

Miller, W.S., Zhuang, L., Bottema, J., Wittebrood, A.J., De Smet, P., Haszler, A., Vieregge, A., 2000. Recent developments in aluminium alloys for the automotive industry. Materials Science and Engineering A 280, 37–49.

Myhr, O.R., Grong, O., Anderson, S.J., 2001. Modelling of the age hardening behaviour of Al-mg-Si alloys. Acta Materialia 49, 65–75.

Polmear, I.J., 2000. Light Alloys – Metallurgy of the Light Metals, third ed. Butterworth–Heinemann, Oxford.

Porter, D.A., Easterling, K.E., 2001. Phase Transformation in Metals and Alloys, second ed. Nelson Thornes Ltd., Cheltenham.

Trivedi, P., Field, D.P., Weiland, H., 2004. Alloying effects on dislocations substructure evolution of aluminium alloys. International Journal of Plasticity 20, 459–476.

Vadasz, P., Vadasz, A.S., 2002. The neoclassical theory of population dynamics in spatially homogeneous environments. (1) Derivation of universal laws and monotonic growth. Physica A: Statistical mechanics and its applications 309 (3–4), 329–359.

Varley, P.C., 1970. The Technology of Aluminium and its Alloys, first ed. Newnes–Butterworths, London.

Vermolen, F.J., Van der Zwaag, S., 1996. A numerical model for the dissolution of spherical particles in binary alloys under mixed mode control. Material Science and Engineering A 220 (1–2), 140–146.

Vermolen, F.J., Vuik, C., 2000. A mathematical model for the dissolution of particles in multi-component alloys. Journal of Computational and Applied Mathematics 126 (1–2), 233–254.

Wu, P.D., Jain, M., Savoiea, J., MacEwen, S.R., Tu cub, P., Neale, K.W., 2003. Evaluation of anisotropic yield functions for aluminium sheets. International Journal of Plasticity 19 (1), 121–138.

Yoon, J.W., Barlat, F., Dick, R.E., Chung, K., Kang, T.J., 2004. Plane stress yield function for aluminium alloy sheets – part II: FE formulation and its implementation. International Journal of Plasticity 20, 495–522.

Zhang, D.L., Zheng, L.H., StJohn, D.H., 2002. Effect of a short solution treatment time on microstructure and mechanical properties of modified Al–7wt.%Si–0.3wt%.Mg alloy. Journal of Light Materials 2 (1), 27–36.